Journal of The Electrochemical Society, **157** (7) B1000-B1007 (2010)
0013-4651/2010/157(7)/B1000/8/$28.00 © The Electrochemical Society

A Durable PEFC with Carbon-Supported Pt–TiO_2 Cathode: A Cause and Effect Study

S. Vinod Selvaganesh,[a] G. Selvarani,[a] P. Sridhar,[a,*] S. Pitchumani,[a] and A. K. Shukla[b,*,z]

[a]*CSIR-Central Electrochemical Research Institute-Madras Unit, CSIR Madras Complex, Taramani, Chennai 600113, India*
[b]*Solid State and Structural Chemistry Unit, Indian Institute of Science, Bangalore 560012, India*

Durability is central to the commercialization of polymer electrolyte fuel cells (PEFCs). The incorporation of TiO_2 with platinum (Pt) ameliorates both the stability and catalytic activity of cathodes in relation to pristine Pt cathodes currently being used in PEFCs. PEFC cathodes comprising carbon-supported Pt–TiO_2 (Pt–TiO_2/C) exhibit higher durability in relation to Pt/C cathodes as evidenced by cell polarization, impedance, and cyclic voltammetry data. The degradation in performance of the Pt–TiO_2/C cathodes is 10% after 5000 test cycles as against 28% for Pt/C cathodes. These data are in conformity with the electrochemical surface area and impedance values. Pt–TiO_2/C cathodes can withstand even 10,000 test cycles with nominal effect on their performance. X-ray diffraction, transmission electron microscope, and cross-sectional field-emission-scanning electron microscope studies on the catalytic electrodes reflect that incorporating TiO_2 with Pt helps in mitigating the aggregation of Pt particles and protects the Nafion membrane against peroxide radicals formed during the cathodic reduction of oxygen.
© 2010 The Electrochemical Society. [DOI: 10.1149/1.3421970] All rights reserved.

Manuscript submitted February 12, 2010; revised manuscript received April 5, 2010. Published May 13, 2010.

Among various fuel cells under active development, polymer electrolyte fuel cells (PEFCs) are especially attractive due to their high efficiency, quick start-up, and low temperature operational flexibility. Although PEFCs are at an advanced stage of development, their operational durability, both for stationary and automotive applications, remains a concern. Accordingly, extensive research and development efforts are presently being pursued to enhance their reliability and durability.

Owing to the slow kinetics of the cathodic reaction and the acidic nature of the membrane electrolyte in PEFCs, generally, noble metals like platinum need to be used as a catalyst. Usually, Pt-metal catalyst is supported on to a high surface area carbon to increase the surface area for the catalyst. However, the activity and long-term stability of Pt remains limited and needs to be enhanced. Generally, the performance deterioration in PEFCs during their long-time operation is attributed partly to the reduction in the active area of the platinum electrocatalyst, usually caused by carbon support corrosion-triggered agglomeration, dissolution, redeposition, and migration of platinum particles onto the membrane electrolyte.[1-4] The alloying of platinum with transition metals shows a high degree of crystallinity and enhanced activity in relation to pristine Pt. Although, the incorporation of transition metal(s) with Pt helps mitigate the aggregation of catalyst particles during long-term operation of PEFCs, the catalyst remains prone to dissolution.[5]

To mitigate the aforesaid problem, the introduction of another noble metal, such as palladium and gold, to Pt matrix has been adopted with fruition; but this becomes cost intensive. Recently, the addition of stable metal oxides such as MOx (M = Ru, W, or Ti) with Pt has also been investigated for enhancing its catalytic activity and stability.[6-14] Among these metal oxide catalysts, TiO_2 being cost-effective and acid stable, is particularly attractive. Brewer and Wengert[15] have argued that the hypo d-electron character of titanium oxide facilitates its interaction with noble metals, like Pt, ameliorating their catalytic activity. This change in the catalytic activity has been explained using Hammer and Norskov's concept,[16] according to which the reactivity alters through the changes in adsorbate interaction energy brought about by a shift in the local d-band position relative to the Fermi level.

In the literature,[6-14] the suitability of TiO_2 as a catalyst support has been explored, and it has high stability in relation to a conventional carbon support. However, the relatively lower electronic conductivity of the former results in an increased ohmic resistance of the cell.[6-8] Recently, electrocatalytic oxygen reduction on carbon-supported Pt–TiO_2 has been reported.[13,14,17-19] TiO_2 also prevents aggregation of the catalyst particles. However, it is important to evaluate the suitability of Pt–TiO_2 and its stability in stringent fuel cell operating conditions, namely high operating potentials, high oxygen concentration, and low pH at cathode.

The loss in surface area of the catalyst and the associated structural changes in the catalyst layer primarily degrade the fuel cell performance, which is particularly of concern when the cell is operated under dynamic load condition, where the cell is cycled at high to low currents with corresponding variation in cell potential between 0.6 and 1 V. Besides, the start-up and shutdown cycles also affect the fuel cell performance. Carbon corrosion in the electrodes is one of the root causes of performance degradation of fuel cells. Carbon corrosion in PEFCs cathodes occurs at high cathode potentials, while start-up/shutdown cycles result in the loss of Pt surface area by particle aggregation.[20-22] Carbon corrosion in PEFC anodes is brought about when the PEFC is operated under fuel-starved condition. In recent years, to simulate fuel cell operating condition with high potential cycling at the cathode, accelerated stress test (AST) is conducted where the cathode is cycled between 0.6 and 1 V.

In the present study, AST has been conducted to evaluate the degradation resistance of PEFC with Pt–TiO_2/C cathode vis à vis a PEFC with a Pt/C cathode. In the literature, a few studies are available for Pt–TiO_2 as a durable catalyst, and it is reported[9,23,24] that the use of TiO_2 as support material shows appreciable electrochemical activity with improved durability. However, the performance of the Pt–TiO_2 cathode is lower by about 100 mV at a load current density of 400 mA/cm^2 as compared to the Pt/C cathode; this is essentially due to the higher resistance of the membrane electrode assembly (MEA) with a TiO_2-based electrocatalyst in relation to the MEA with carbon-based electrocatalyst.[9] Tian et al.[25] have also reported that Pt–TiO_x/C as a cathode catalyst exhibits improved durability in relation to Pt/C cathode catalyst. However, the durability study is performed by loading the test cell galvanostatically at 500 mA/cm^2 for 14 h followed by keeping the cell at open-circuit potential (OCP) for 10 h with repeated cycling over 580 h.

In the literature,[22,26-44] various degradation modes for PEFCs have been discussed and some modeling studies based on the effect of aging and dynamics of degradation are reported. In the present study, a detailed test protocol due to the U.S. Department of Energy (DoE) is adopted with some modification for a better insight on the catalyst degradation. DoE protocols are intended to establish a common approach for determining and projecting the durability of various PEFC components under simulated automotive drive cycle conditions.

* Electrochemical Society Active Member.
z E-mail: akshukla2006@gmail.com

Downloaded 22 Jun 2010 to 210.212.252.226. Redistribution subject to ECS license or copyright; see http://www.ecsdl.org/terms_use.jsp

The adopted test protocol includes potential cycling of PEFCs between 0.6 and 1 V vs dynamic hydrogen electrode (DHE) in conformity with the cell operating voltage range and open-circuit voltage conditions. The potential range is effective for fuel cell vehicles as it simulates the dynamic load cycling. In the present study, the performance loss in PEFCs is assessed through galvanostatic polarization and in situ cyclic voltammetry (CV), and ohmic resistance and polarization resistance values are estimated from impedance measurements on the cells. The degradation behavior of the membrane is also analyzed by measuring the fluoride-ion emission from the cathode outlet of the cell. Powder X-ray diffraction (XRD) and transmission electron microscopy (TEM) are used to determine the catalyst crystallinity and morphology, and the changes in membrane and catalyst-layer structures are determined through cross-sectional images of MEAs using field-emission-scanning electron microscopy (FESEM).

Experimental

Preparation of Pt–TiO_2/C catalyst.— Pt–TiO_2 catalyst was prepared by a sol–gel route reported elsewhere.[18] In brief, the required amount of titanium iso-propoxide (Aldrich) was diluted with isopropanol and made into a homogeneous solution by ultrasonication. Titania sol was obtained by adding 0.5 M aqueos H_2SO_4 to titanium iso-propoxide solution accompanied with ultrasonication for 1 h. Finally, the required quantity of carbon-supported Pt (40 w/o from Alfa Aesar) was added with continuous stirring. The resultant mixture was left for 24 h to form a gel and subsequently heated at 80°C for 1 h to remove all volatile substances present in it. The resulting cake was pulverized and subjected to heat-treatment at 750°C in a flowing mixture of 90% N_2–10% H_2 for 5 h and was cooled to room temperature; the heat-treated sample is represented as 750Pt–TiO_2/C. In the present study, 750Pt–TiO_2/C with Pt to Ti in 2:1 atomic ratio have been employed. In the manuscript, carbon-supported platinum heat-treated at 750°C is represented as 750 Pt/C while pristine platinum catalyst is represented as Pt/C.

Fabrication of MEAs.— MEAs were fabricated as described elsewhere.[45] In brief, both the anode and the cathode comprised a backing layer, a gas diffusion layer and a catalyst layer. A Teflonized (15 w/o PTFE) carbon paper (Toray TGP-H-120) of 0.35 mm thickness was employed as the backing layer in these electrodes. To prepare the gas diffusion layer, a Vulcan XC72R carbon was suspended in cyclohexane and agitated in an ultrasonic water bath for 40 min. To this, 15 w/o PTFE suspension was added with continuous agitation. The resultant slurry was spread onto a Teflonized carbon paper and sintered in a furnace at 350°C for 30 min.

To prepare the catalyst layer, the required amount of the catalyst (Pt/C or 750 Pt/C or 750 Pt–TiO_2/C) was suspended in isopropyl alcohol and the mixture was agitated in an ultrasonic water bath, and 7 and 30 w/o of Nafion (DuPont) dispersion was added to the anode and cathode slurry, respectively, with continuous ultrasonication for 1 h. Pt/C was used for the anode preparation. The resultant ink was coated onto the gas diffusion layer of the respective electrodes. Both the anode and cathode contained a platinum loading of 0.5 mg cm^{-2} (active area 25 cm^2), which was kept constant in all the MEAs. To establish effective contact between the catalyst layer and the polymer electrolyte, a thin layer of Nafion dispersion (5 w/o) diluted with isopropyl alcohol in 1:1 ratio was spread onto the surface of each electrode. MEAs were obtained by hot-pressing the cathode and anode on either side of a pretreated Nafion 1135 membrane at 60 kg cm^{-2} at 130°C for 3 min.

Electrochemical characterization.— Cell polarization studies.— Cell equilibration and polarization protocols for MEAs were similar to those recommended by the DoE.[46] MEAs were evaluated using a conventional 25 cm^2 fuel cell fixture with a parallel serpentine flow field machined on graphite plates obtained from M/s Schunk Kohlenstofftechnik GmbH, Germany. After equilibration, galvanostatic polarization data for the cells were obtained at 60°C at varying load current densities at recommended stoichiometries of hydrogen and oxygen feeds at atmospheric pressure at the anode and cathode, respectively, using an LCN100-36 electronic load procured from Bitrode Corporation.

ESA measurements.— CV measurements were conducted around ~25°C to determine the H_{ad}/H_{de} charge for PEFC cathodes using a potentiostat (Autolab PGSTAT 30) with its lead for the working electrode connected to the cell cathode, and the leads for the reference and counter electrodes connected to the cell anode.[45] During the experiment, humidified hydrogen (3 stoichiometry) at 0.8 A/cm^2 and nitrogen at a flow rate of 25 mL/min were fed to the anode and cathode, respectively. Voltammograms were recorded between 0 and 1 V (vs DHE) at a sweep rate of 50 mV/s at room temperature. Cycles were repeated until stable and reproducible voltammograms were obtained. The region between 0.0 and 0.4 V, corresponding to the hydrogen adsorption/desorption region, was used to measure the electrochemical surface area (ESA) of the catalyst. The ESA of the Pt catalyst was estimated from Eq. 1 given below[47]

$$\mathrm{ESA}(\mathrm{cm}^2/\mathrm{g}_{\mathrm{Pt}}) = \frac{Q_{\mathrm{H}}(\mu\mathrm{C}/\mathrm{cm}^2)}{210(\mu\mathrm{C}/\mathrm{cm}^2) \times L(\mathrm{g}_{\mathrm{Pt}}/\mathrm{cm}^2)} \quad [1]$$

where Q_H represents the charge of hydrogen adsorption/desorption and is taken as 210 $\mu C/cm^2$ to oxidize/reduce a monolayer of H_2 on smooth platinum surface and L is the loading of platinum in g/cm^2.

Electrochemical potential cycling.— During electrochemical potential cycling, the cell was fed with humidified hydrogen at the anode and nitrogen at the cathode with gas flow rates similar to ESA measurements at 65°C using a potentiostat (Autolab PGSTAT 30) with its leads for the reference and counter electrodes connected to the cell anode and its lead for working electrode connected to the cell cathode. AST was conducted by cycling the cell between 0.6 and 1 V at a scan rate of 20 mV/s. The cell polarization and CV for measuring the ESA were conducted for every 500 AST cycles. MEAs subjected to AST were examined by XRD, TEM, and cross-sectional FESEM. Fluoride concentration was determined in the water from the cathode exhaust after completion of AST.

Ac impedance measurements.— A frequency response analyzer (Autolab PGSTAT 30) was used to measure the polarization resistance of the MEAs at OCP and at the operating cell voltage of 0.6 V. The reference and counter electrode leads were connected to the hydrogen electrode, and the working electrode lead was linked to the air electrode. Impedance measurements were conducted in the frequency range between 5 kHz and 100 mHz by imposing a single sinusoidal wave with an amplitude of 10 mV.

Physical characterization.— XRD studies.— Powder XRD studies were conducted to analyze the change in crystallinity and particle size of Pt particles in Pt/C, 750Pt/C, and 750Pt–TiO_2/C before and after AST. For this purpose, samples were scraped from the cathode of the MEAs after AST, and their powder XRD patterns were obtained on a Philips X'Pert diffractometer using Cu Kα radiation (λ = 1.5406 Å) between 20 and 80° in reflection geometry in steps of 0.034°/min. The particle size of Pt was calculated by an X-ray line broadening technique employing Debye–Scherer equation[18]

$$t = \frac{0.89 \times \lambda}{\beta \times \cos\ \theta} \quad [2]$$

In Eq. 2, t is the particle diameter (in Å), λ is the wavelength of radiation (in Å), β is the full width at half-maximum (in radian), and θ is the Bragg diffraction angle (in degrees).

XPS.— X-ray photoelectron spectrometry (XPS) for catalysts was recorded on a MultiLab 2000 (Thermofisher Scientific, U.K.) X-ray photoelectron spectrometer fitted with a twin anode X-ray source using Mg Kα radiation (1253.6 eV). For recording the desired spectrum, powder sample was pressed onto a conducting carbon tape pasted onto the indium-coated stainless steel stubs. The sample stubs were initially kept in the preparatory chamber overnight at 10–9

Downloaded 22 Jun 2010 to 210.212.252.226. Redistribution subject to ECS license or copyright; see http://www.ecsdl.org/terms_use.jsp

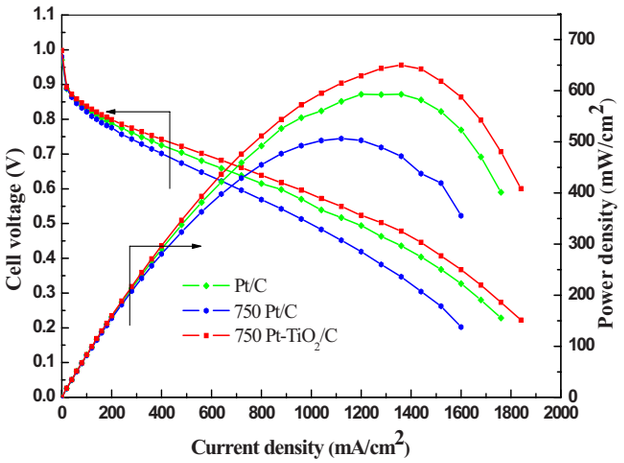

Figure 1. (Color online) Steady-state performance curve for PEFCs with Pt/C, 750 Pt/C, and 750 Pt–TiO_2/C cathodes before AST.

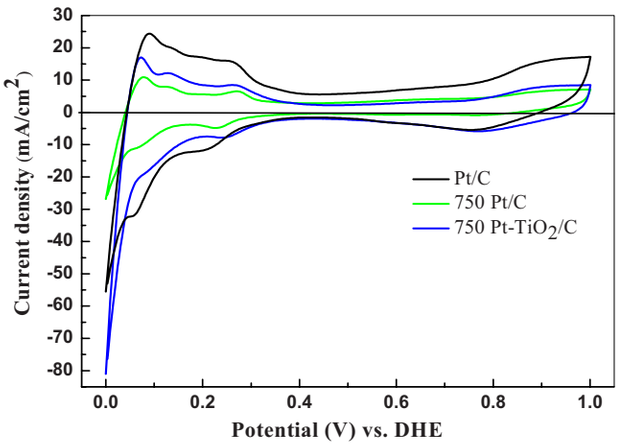

Figure 2. (Color online) Cyclic voltammogram for PEFCs with Pt/C, 750 Pt/C, and 750 Pt–TiO_2/C cathodes prior AST at 50 mV/s.

mbar for desorbing any volatile species and were introduced into the analysis chamber at 9.8×10^{-10} mbar for recording the spectra.

TEM analysis.— TEM was used to determine the changes in the average particle size of Pt before and after AST in Pt/C, 750Pt/C, and 750Pt–TiO_2/C catalysts. For this purpose, the samples were scraped from the cathode of the MEAs after AST. The microscopic features of the samples were examined by using a TCNAI 20 G2 transmission electron microscope (200 kV) by suspending them in isopropyl alcohol and casting by dropping the suspension onto a carbon-coated copper grid followed by solvent evaporation in vacuum at room temperature.

Cross-sectional FESEM analysis.— Cross-sectional views of the MEAs before and after AST were obtained through FESEM using a field-emission-scanning electron microscope (FEI-Quanta, F200). For this purpose, all the MEAs were dried at 50°C for 5 h after which a small portion of MEA was divided and mounted on a copper grid for cross-sectional SEM observation.

Fluoride-ion measurements.— The concentration of fluoride ions from the cathode of the MEAs after AST was estimated by using fluoride ion-selective electrode (Thermo Scientific Orion Star Series meter). Before conducting the measurement, the effluent water was standardized by using a TISAB-III standard solution.

Results and Discussion

The polarization curves for PEFCs with Pt/C, 750Pt/C, and 750Pt–TiO_2/C cathodes using hydrogen and oxygen as fuel and oxidant, respectively, are depicted in Fig. 1. The PEFC with a 750Pt–TiO_2/C cathode exhibits enhanced performance in relation to the PEFCs with Pt/C or 750 Pt/C cathodes. The ameliorated performance for the PEFC with a 750Pt–TiO_2/C cathode is attributed to the influence of TiO_2 on the catalytic activity of Pt brought about by the electronic interactions between platinum and the metal oxide as visualized in the light of hyper-d-electron character of Pt and hypo-d-electron character of TiO_2.[15,48] According to the electrocatalytic theory based on hypo–hyper-d-interionic interactions, the interacting effect brings about an improvement in the Pt electrode as the change in the surface d-state affects the interaction between the adsorbate valence states and the metal surface resulting in an increase in the number of active sites for absorption of oxygen species. Besides, the metal oxide in the catalyst increases the reduction potential of the oxide formed on the surface of the platinum.[22] Moreover, the enhanced dispersion of Pt catalyst particles due to reduced aggregation in the presence of TiO_2 during annealing also helps increasing the catalytic activity of 750Pt–TiO_2/C.

CV has been conducted to measure the ESA for Pt/C, 750Pt/C, and 750Pt–TiO_2/C, and the voltammograms are presented in Fig. 2. All the catalysts show peaks between 0.05 and 0.25V (vs DHE) corresponding to hydrogen adsorption/desorption followed by the double-layer region. At potentials >0.65 V (vs DHE), platinum oxidation/reduction region is observed. The charge associated with hydrogen adsorption/desorption (H_{ad}/H_{de}) for 750Pt/C is lesser than that for Pt/C, possibly due to particle aggregation during heat-treatment.[11] 750Pt–TiO_2/C shows a higher H_{ad}/H_{de} charge than 750Pt/C, which could be attributed to the hindrance of Pt particles aggregation by amorphous titanium oxide as reflected by TEM and powder XRD studies. However, charges associated with H_{ad}/H_{de} for 750 Pt/C and 750Pt–TiO_2 are lesser than Pt/C, possibly due to the increased particle size during heat-treatment of the catalysts.

As already shown from the polarization studies in Fig. 1, 750Pt–TiO_2/C performs better in relation to both Pt/C and 750Pt/C but the performance of 750 Pt/C is far lower than Pt/C. Because Pt/C is the conventional catalyst for fuel cells, both Pt/C and 750Pt–TiO_2/C catalysts have been tested for their durability. To evaluate the stability of Pt/C and 750Pt–TiO_2/C catalysts, AST is conducted. Generally, the AST protocol of potential cycling is used for the evaluating catalyst durability.[47,49]

During these studies, humidified hydrogen and nitrogen are fed to the anode and cathode, respectively. Subsequently, the cathode is cycled between 0.6 and 1 V (vs DHE) at 65°C. During the study, the exhaust from the cathode is collected for fluoride-ion analysis. The changes in cell performance, ESA, and polarization resistance are monitored for every 500 cycles. The PEFC comprising a 750Pt–TiO_2/C cathode exhibits a relatively less performance loss suggesting enhanced stability in relation to PEFCs with Pt/C cathode. Galvanostatic polarization curves for PEFCs with 750Pt–TiO_2/C and Pt/C cathodes are presented in Fig. 3a and b before and after 5000 cycles. Deterioration in performance of the PEFC with a Pt/C cathode is 28% after 5000 cycles in relation to 10% of the PEFC with a 750Pt–TiO_2/C cathode.

Loss in ESA for the Pt/C and 750Pt–TiO_2/C catalysts is monitored for every 500 cycles. The comparative cyclic voltammograms for 750Pt–TiO_2/C and Pt/C before and after 5000 cycles are presented in Fig. 4a and b. The data shows that the TiO_2-incorporated cathode exhibits a 6% loss in ESA after AST, while it is as high as 25% for Pt/C. These data agree well with cell polarization data. From cell polarization and CV studies, the amorphous titanium oxide not only ameliorates the catalytic activity of Pt but also clearly resists the Pt particles aggregation.

Impedance studies are also conducted both at OCP and 0.6 V for PEFCs with 750Pt–TiO_2/C and Pt/C cathodes. The Nyquist plots for PEFCs with Pt/C and 750Pt–TiO_2/C cathodes before and after 5000 cycles are shown in Fig. 5a and b. The ohmic resistance (R_s) values

Downloaded 22 Jun 2010 to 210.212.252.226. Redistribution subject to ECS license or copyright; see http://www.ecsdl.org/terms_use.jsp

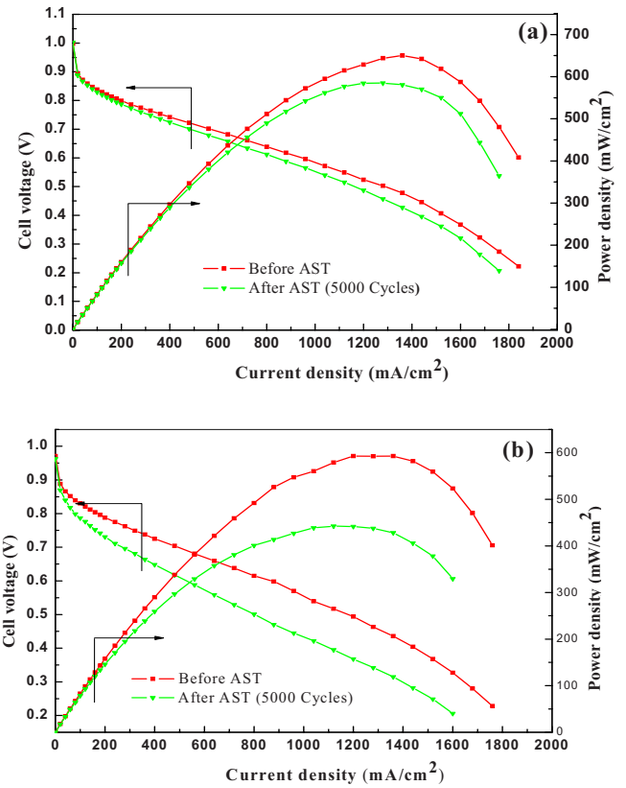

Figure 3. (Color online) Steady-state performance curve for PEFCs with (a) 750Pt–TiO_2/C and (b) Pt/C cathodes before and after 5000 potential cycles.

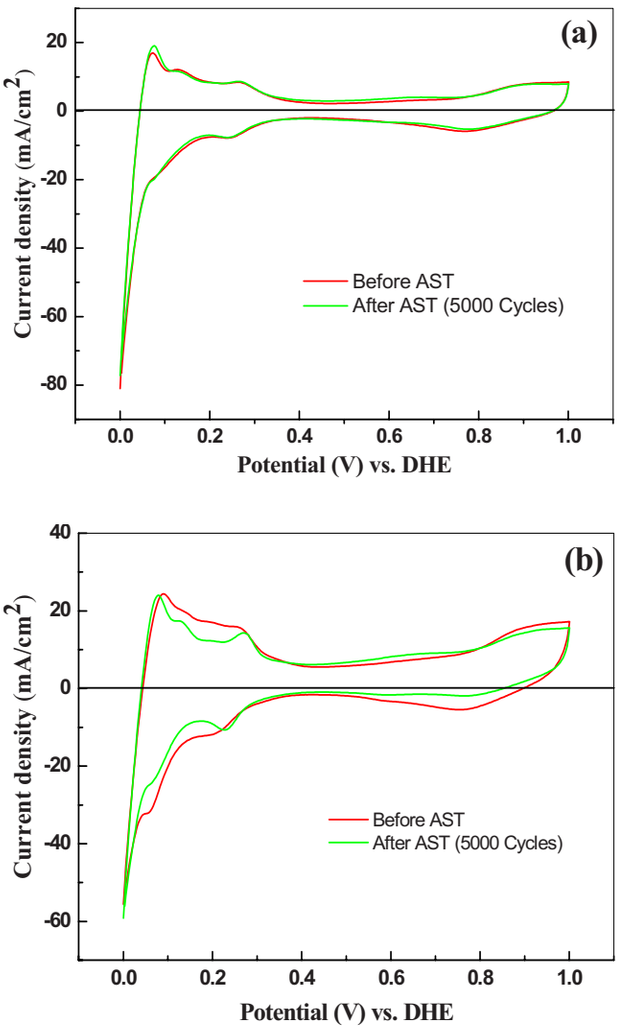

Figure 4. (Color online) Cyclic voltammogram for PEFCs with (a) 750Pt–TiO_2/C and (b) Pt/C cathodes before and after 5000 potential cycles at 50 mV/s.

for PEFCs with 750Pt–TiO_2/C and Pt/C cathodes are almost similar before AST studies at OCP and 0.6 V. However, the charge-transfer resistance (R_{ct}) at 0.6 V is lower for the PEFC with a 750Pt–TiO_2/C cathode in relation to that for the PEFC with a Pt/C cathode. The lower charge-transfer resistance appears to be responsible for the higher catalytic activity of 750Pt–TiO_2/C. The ohmic resistance for the PEFC with a 750Pt–TiO_2/C cathode shows little change after 5000 and even 10,000 cycles, while the PEFC with a Pt/C cathode shows a distinct effect, as depicted in Fig. 5b. Also, the R_{ct} value for the PEFC with a Pt/C cathode after 5000 cycles is much higher in relation to R_{ct} for PEFC with 750Pt–TiO_2/C cathode.

Although the PEFC with a 750Pt–TiO_2/C cathode shows higher performance and durability up to 5000 potential cycles in relation to the PEFC with Pt/C cathode, the AST test is continued beyond 5000 cycles. The PEFC with a 750Pt–TiO_2/C cathode remains stable with performance loss of only 7% while cycling between 5000 and 10,000 cycles. By contrast, the test had to be terminated after 6000 cycles for the PEFC with Pt/C cathode. The performance curves for the PEFC with a 750Pt–TiO_2/C cathode before and after 10,000 cycles are depicted in Fig. 6 and the comparative cyclic voltammograms for the PEFC with 750Pt–TiO_2/C before and after 10,000 cycles are presented in Fig. 7. To correlate the loss in cell performance with loss in ESA for the PEFCs with Pt/C and 750Pt–TiO_2/C cathodes for every 1000 cycles, comparative cell polarization data and ESA values are presented in Fig. 8. The cell performance and ESA values fall sharply in the PEFC with a Pt/C cathode while the values decay slowly for the PEFC with a 750Pt–TiO_2/C cathode. These results clearly reflect the influence on the durability of the Pt/C cathode due to incorporation of TiO_2.

Electrochemical characterization studies, namely cell polarization, ESA, and impedance measurements, suggest enhanced performance and durability of the PEFC with Pt–TiO_2/C cathode in relation to the PEFC with bare Pt/C cathode. To ascertain the role of TiO_2 in Pt–TiO_2/C, ex situ physical characterization studies, namely, powder XRD, TEM, and cross-sectional FESEM, are carried out on the catalyst after AST and compared with those obtained for it before AST. Powder XRD patterns for Pt/C, 750Pt/C, and 750Pt–TiO_2/C cathodes before and after AST are shown in Fig. 9. XRD patterns for Pt/C, 750Pt/C, and 750Pt–TiO_2/C show peaks corresponding to (111), (200), (220), (311), and (222) planes that are characteristic of a face-centered cubic structure of Pt. The diffraction peaks for 750Pt/C and 750Pt–TiO_2/C catalyst are sharper than those for Pt/C catalyst even before AST indicating larger particle size due to Pt aggregation during heat-treatment. These data agree well with the data obtained from CV and TEM studies. Mean particle size for Pt particles in Pt/C and 750Pt–TiO_2/C before and after AST are calculated from the full width at half-maximum value of the (111) peak using the Debye–Scherrer equation. In addition, the mean particle size of Pt in 750 Pt/C before AST is also obtained. The mean particle size values for Pt particles in Pt/C, 750 Pt/C, and 750Pt–TiO_2/C before AST are 4, 19, and 13 nm, respectively. After AST, the mean particle size values of Pt particles in Pt/C and 750Pt–TiO_2/C are 26 and 16 nm, respectively. The increased particle size is attributed to catalyst particles aggregation during the potential cycling. The disproportionate increase in Pt particle size confirms that the TiO_2 inhibits Pt particle agglomeration.

Downloaded 22 Jun 2010 to 210.212.252.226. Redistribution subject to ECS license or copyright; see http://www.ecsdl.org/terms_use.jsp

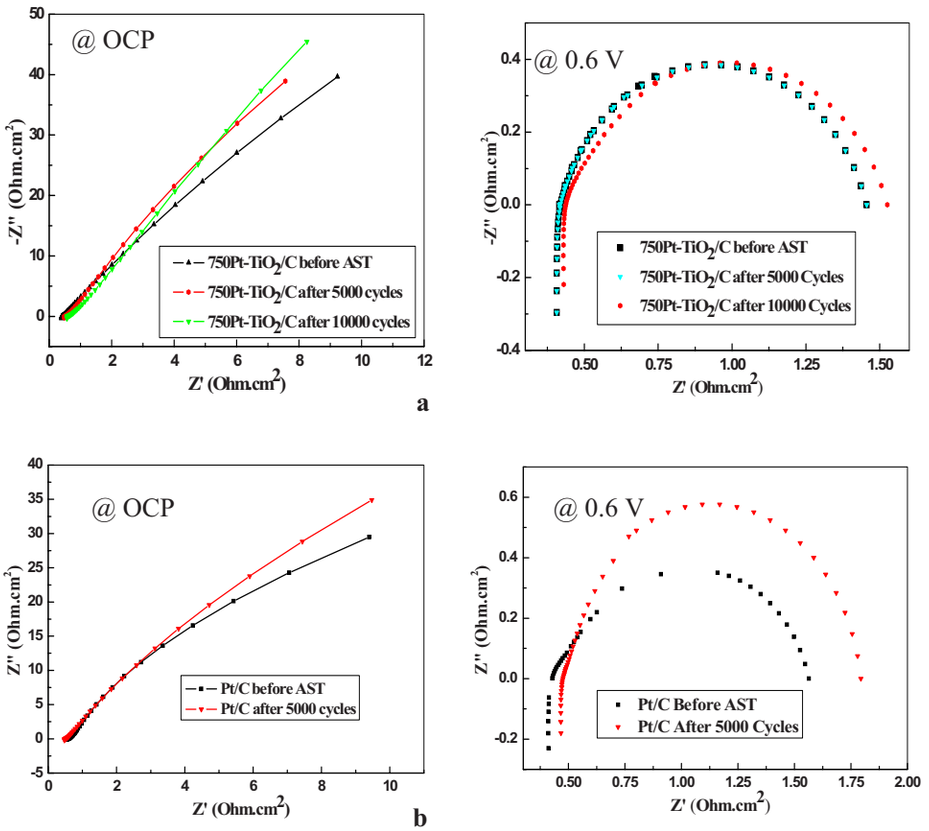

Figure 5. (Color online) Nyquist plots for PEFCs with (a) 750Pt–TiO_2/C and (b) Pt/C before and after AST at OCP and 0.6 V.

XPS is a useful technique to analyze the surface oxidation states of catalyst materials. Accordingly, to gather the information on the oxidation states of Pt in various catalysts, XPS are recorded for Pt/C and 750Pt–TiO_2/C (2:1) catalysts. Pt (4f) spectra for Pt/C, 750 Pt/C, and 750Pt–TiO_2/C (2:1) are not shown for the sake of brevity as these are similar with little change in binding energy values for all the three samples. Hence, Ti in Pt–TiO_2/C is expected to be present only in the oxidized state. To examine the exact oxidation state of Ti in 750Pt–TiO_2/C (2:1), the XPS is recorded for the Ti (2p) region, as shown in Fig. 10. In the spectrum, two peaks are observed at binding energies 458.7 and 465 eV, which are attributed to Ti $(2p_{3/2})$ and Ti $(2p_{1/2})$, respectively.[18] Accordingly, the data confirm the presence of Ti in 750Pt–TiO_2/C (2:1) as Ti^{4+}.

TEM images for Pt/C and 750Pt–TiO_2/C catalysts before and after AST are shown in Fig. 11. Nanoparticles of Pt are well dispersed on the carbon support with a narrow particle size distribution for Pt/C catalyst. In 750Pt–TiO_2/C, the amorphous titanium oxide is barely visible due to high platinum loading on carbon. However, platinum is homogeneously dispersed on carbon. The Pt particles are quite large in 750Pt–TiO_2/C in relation to Pt/C, which is due to the heat-treatment for the former. For the sake of comparison, the TEM of 750 Pt/C is also included. The particle size of Pt in 750Pt/C is larger than that in 750Pt–TiO_2/C. The Pt particle size in Pt/C increases significantly after AST compared to that in 750Pt–TiO_2/C; the increased particle size during AST agreeing well with the conclusions derived from powder XRD and CV studies. After AST, the Pt particle size in Pt/C is much larger than that in 750 Pt/C before

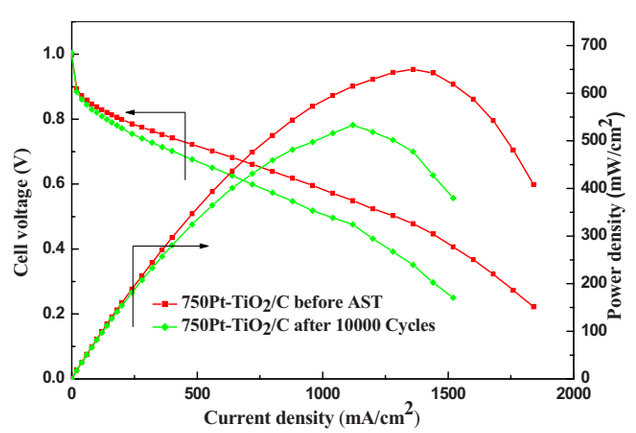

Figure 6. (Color online) Steady-state performance curves for PEFCs with 750Pt–TiO_2/C cathode before and after 10,000 potential cycles.

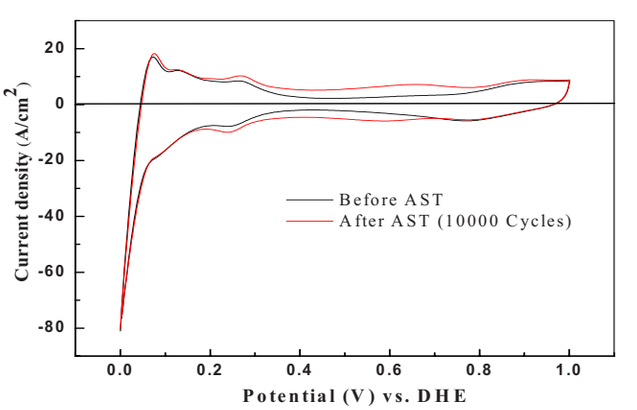

Figure 7. (Color online) Cyclic voltammogram for PEFCs with 750Pt–TiO_2/C cathode before and after 10,000 potential cycles at 50mV/s.

Downloaded 22 Jun 2010 to 210.212.252.226. Redistribution subject to ECS license or copyright; see http://www.ecsdl.org/terms_use.jsp

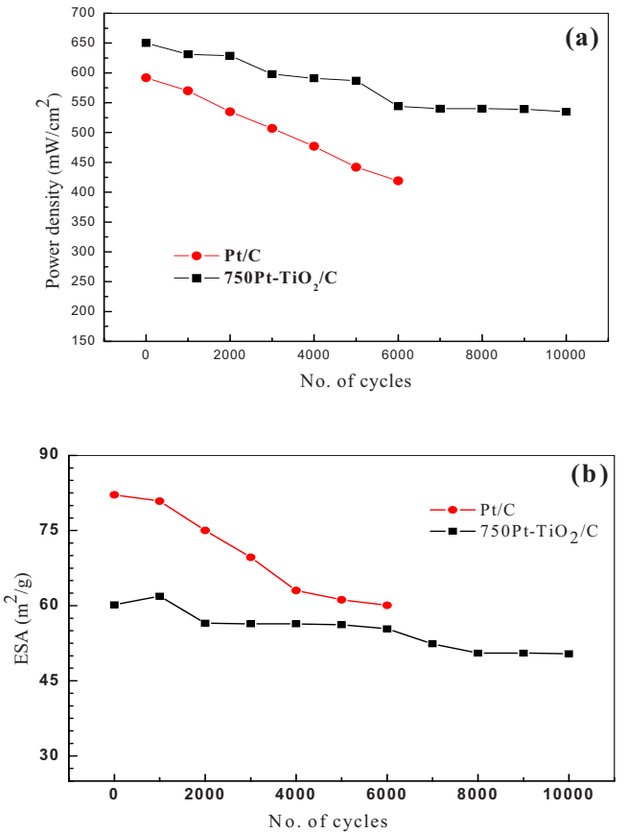

Figure 8. (Color online) Change in (a) steady-state performance and (b) ESA with accelerated potential cycles.

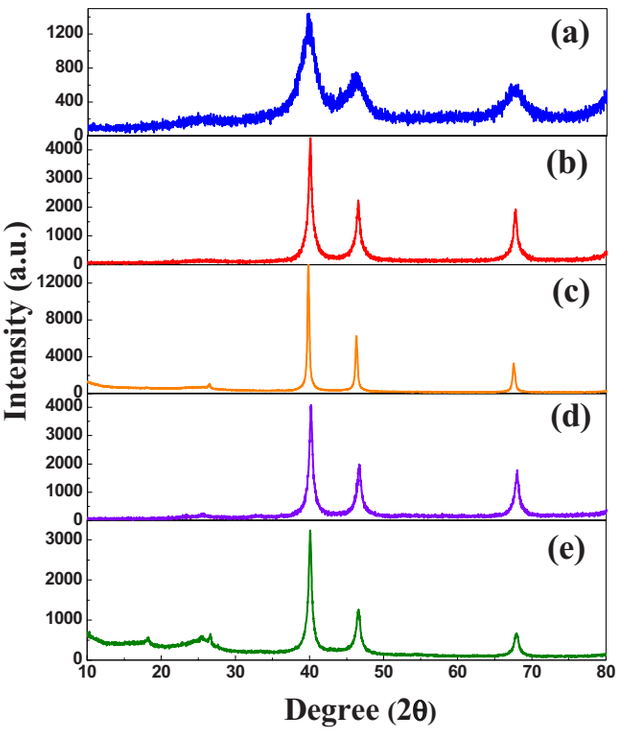

Figure 9. (Color online) Powder XRD patterns for (a) Pt/C, (b) 750Pt/C, (c) Pt/C after AST, (d) 750Pt–TiO_2/C, and (e) 750Pt–TiO_2/C after AST.

AST. Generally, the smaller particles of Pt have a high tendency to agglomerate during AST because of their high surface energy, whereas once particles have grown up to a certain level, the agglomeration rate tends to come down. In the present system, the initial particle size of Pt in Pt/C is around 3 nm while it is 9 nm in 750Pt–TiO_2. However, after AST study the Pt particle in Pt/C grows up to 23 nm, whereas it remains limited to 13 nm in 750Pt–TiO_2/C. In addition, the Pt particle size in 750 Pt/C is around 20 nm before AST, which is lesser than that for Pt/C after AST. Hence, TiO_2 hinders Pt particles agglomeration. In 750Pt–TiO_2/C, both the larger particle size of Pt and the presence of TiO_2 are responsible for the stability during the AST. TiO_2 induces a strong metal support interaction (SMSI) preventing the corrosion of both catalyst particles as well as the carbon support.[50] According to Neophytides et al.,[48] the increase in the electrocatalytic activity of the Pt–TiO_2 catalyst is due to the synergistic activity of the hypo–hyper-d-interelectronic bonding between noble metal and transition-metal oxides; the latter resulting in SMSI. Indeed, the core of such an SMSI support interaction, almost without any exception, lies in the Brewer hypo–hyper-d-interelectronic bonding effect resulting in interactive properties,[51] which is further substantiated by Jaksic[52] and Tauster et al.,[53] who have discussed the enhanced catalytic activity of Pt–TiO_2 catalyst in the light of an oxygen reduction reaction (ORR) mechanism. The typical ORR pathways on a noble metal (M) are given below

$$O_2 + M + H_3O^+ + e^- \rightarrow M\text{–}OOH + H_2O \quad [3]$$

$$M\text{–}OOH + M \rightarrow M\text{–}OH + M = O \quad [4]$$

$$M\text{–}OH + M = O + 3H_3O + + 3e^- \rightarrow 5H_2O + 2M \quad [5]$$

The adsorbed primary oxide (M–OH) is considered to be the rate-determining factor in ORR. It is documented that the reversible reaction of the anodic primary oxide formation and its cathodic reduction on hypo-d-oxide supports, under wet conditions, result in an unlimited source of M–OH. The continuous "pumping" effect for the primary oxide effusion or the spillover continuously is known in the SMSI hypo-d-oxide catalytic supports. Accordingly, TEM images clearly reflect poor stability of small Pt particles in Pt/C due to dissolution/sintering under dynamic cycling of the PEFC with Pt/C cathode.

Cross-sectional field-emission scanning electron micrographs for MEAs comprising Pt/C and 750Pt–TiO_2/C cathodes before and after AST are shown in Fig. 12. The magnified cross-sectional micrographs clearly reflect the changes in the catalyst layer as well as in the membrane after AST. The Pt/C catalyst layer undergoes higher

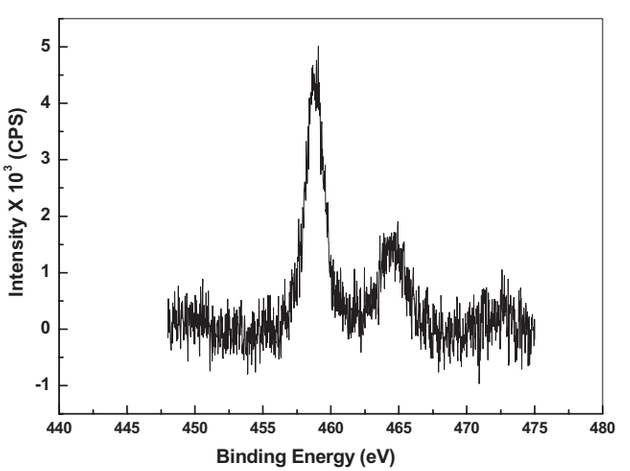

Figure 10. X-ray photoelectron spectra for Ti (3p) region in 750Pt–TiO_2/C (2:1) catalyst.

Downloaded 22 Jun 2010 to 210.212.252.226. Redistribution subject to ECS license or copyright; see http://www.ecsdl.org/terms_use.jsp

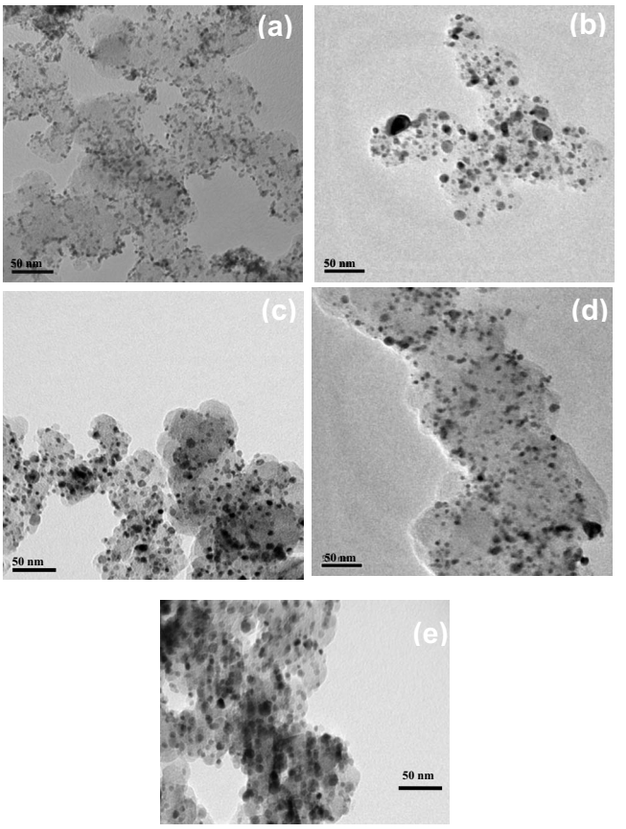

Figure 11. Transmission electron micrographs for (a) Pt/C, (b) Pt/C after AST, (c) 750Pt–TiO_2/C, (d) 750Pt–TiO_2/C after AST, and (e) 750Pt/C.

deformation after AST in relation to 750Pt–TiO_2/C. Besides, a larger variation in membrane thickness for the PEFC with a Pt/C cathode is observed, which may be attributed to the ionomer degradation initiated by $HO^{\bullet}$ and $HO_2^{\bullet}$ originating from hydrogen peroxide generated during the incomplete reduction of oxygen as proposed by Curtin et al.[54] By contrast, in the PEFC with 750Pt–TiO_2/C cathode, only a little variation in the thickness of the membrane after AST is observed due to assimilation of the peroxy radicals by TiO_2.[55] Tengvall et al.[56] have discussed the role of TiO_2 in the elimination of peroxy radicals. It is suggested that TiO–OH matrix traps the superoxide radicals such that little or only a little amounts of free hydroxyl radicals become available for further reactions.

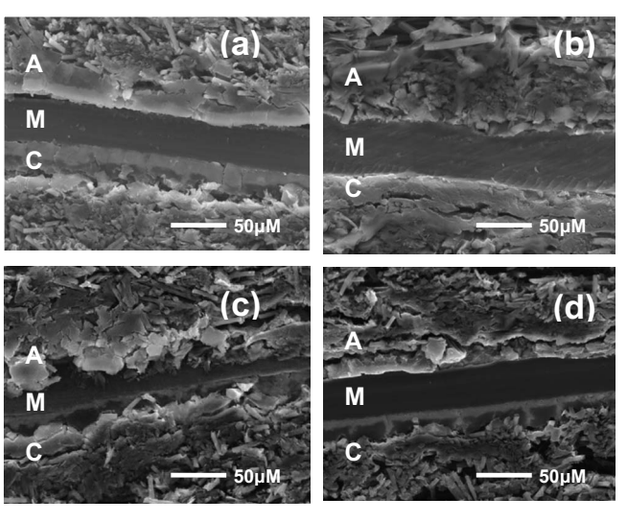

Figure 12. Cross-sectional FESEM micrographs for MEAs in PEFCs with (a) Pt/C, (b) 750Pt–TiO_2/C, (c) Pt/C after AST, (d) 750Pt–TiO_2/C after AST. In the figure, A = anode, M = membrane, and C = cathode.

To study the membrane degradation behavior, F^- ion content is measured from the cathode exhausts of cells using fluoride-ion selective electrode. Fluoride emission rates from cathodes are obtained for PEFCs with Pt/C and 750Pt–TiO_2/C cathodes during AST. The concentration of fluoride ion from the PEFC with a Pt/C cathode is nearly twice to that for the PEFC with a 750Pt–TiO_2/C cathode after 5000 potential cycles. These findings agree with the ac impedance data. Accordingly, TiO_2 incorporation appears to hinder not only the Pt particle aggregation but also helps protect the Nafion membrane against peroxy radicals.

Conclusions

The study suggests that (*i*) the introduction of amorphous TiO_2 to platinum (Pt) ameliorates the catalyst stability in conjunction with its catalytic activity, (*ii*) the degradation in performance of PEFCs with a 750Pt–TiO_2/C cathode is 10% after 5000 potential cycles in relation to 28% for the PEFCs with a Pt/C cathode, (*iii*) PEFCs with 750Pt–TiO_2/C cathode exhibit enhanced durability even up to 10,000 potential cycles with only a little loss in performance in relation to PEFCs with Pt/C cathode that degrade after 6000 potential cycles, and (*iv*) TiO_2 in Pt not only helps mitigate the aggregation of Pt particles but also protects the Nafion electrolyte against peroxide radicals originating from hydrogen peroxide generated during the incomplete reduction of oxygen.

Acknowledgments

Financial support from CSIR, New Delhi through a suprainstitutional project under EFYP is gratefully acknowledged.

CSIR-Central Electrochemical Research Institute assisted in meeting the publication costs of this article.

References

1. M. S. Wilson, F. H. Garzon, K. E. Sickafus, and S. Gottesfeld, *J. Electrochem. Soc.*, **140**, 2872 (1993).
2. M. Schulze, A. Schneider, and E. Gulzow, *J. Power Sources*, **127**, 213 (2004).
3. J. Xie, D. L. Wood, K. L. More, P. Atanassov, and R. L. Borup, *J. Electrochem. Soc.*, **152**, A1011 (2005).
4. D. A. Stevens and J. R. Dahn, *Carbon*, **43**, 179 (2005).
5. M. Pourbiax, *Atlas of Electrochemical Equilibria*, Pergamon Press, Oxford (1966).
6. T. Ioroi, Z. Siroma, N. Fujiwara, S. I. Yamazaki, and K. Yasuda, *Electrochem. Commun.*, **7**, 183 (2005).
7. J. M. Chen, L. S. Sarma, C. H. Chen, M. Y. Cheng, S. C. Shih, G. R. Wang, D. G. Liu, J. F. Lee, M. T. Tang, and B. J. Hwang, *J. Power Sources*, **159**, 29 (2006).
8. J. Shim, C. R. Lee, H. K. Lee, J. S. Lee, and E. J. Cairns, *J. Power Sources*, **102**, 172 (2001).
9. N. Rajalakshmi, N. Lakshimi, and K. S. Dhathathreyan, *Int. J. Hydrogen Energy*, **33**, 7521 (2008).
10. Y. Fu, Z. D. Wei, S. G. Chen, L. Li, Y. C. Feng, Y. Q. Wang, and M. J. Liao, *J. Power Sources*, **189**, 982 (2009).
11. H. J. Kim, D. Y. Kim, H. Han, and Y. G. Shul, *J. Power Sources*, **159**, 484 (2006).
12. L. Xiong and A. Manthiram, *Electrochim. Acta*, **49**, 4163 (2004).
13. H. Song, X. Qiu, X. Li, F. Li, W. Zhu, and L. Chen, *J. Power Sources*, **170**, 50 (2007).
14. M. Gustavsson, H. Ekstrom, P. Hanarp, L. Eurenius, G. Lindbergh, E. Olsson, and B. Kasemo, *J. Power Sources*, **163**, 671 (2007).
15. L. Brewer and P. R. Wengert, *Metall. Trans.*, **4**, 83 (1973).
16. B. Hammer and J. K. Norskov, *Adv. Catal.*, **45**, 71 (2000).
17. G. Kokkinidis, D. Stoychev, V. Larzarov, A. Papoutsis, and A. Milchev, *J. Electroanal. Chem.*, **511**, 20 (2001).
18. G. Selvarani, S. Maheswari, P. Sridhar, S. Pitchumani, and A. K. Shukla, *J. Electrochem. Soc.*, **156**, B1354 (2009).
19. G. Selvarani, S. Maheswari, P. Sridhar, and S. Pitchumani, in *Proceedings of Third European Fuel Cell Technology & Applications Conference*, "Piero Lunghi Conference," Rome, Italy, p. 173 (2009).
20. R. L. Borup, J. R. Davey, F. H. Garzon, D. L. Wood, and M. A. Inbody, *J. Power Sources*, **163**, 76 (2006).
21. P. J. Ferreira, G. J. la O, Y. Shan-Horn, D. Morgan, R. Makharia, S. kocha, and H. A. Gasteiger, *J. Electrochem. Soc.*, **152**, A2256 (2005).
22. K. Kinoshita, *J. Electroanal. Chem. Interfacial Electrochem.*, **48**, 157 (1973).
23. S. Y. Huang, P. Ganesan, S. Park, and B. N. Popov, *J. Am. Chem. Soc.*, **131**, 13898

Downloaded 22 Jun 2010 to 210.212.252.226. Redistribution subject to ECS license or copyright; see http://www.ecsdl.org/terms_use.jsp

(2009).
24. S. Sambandam, V. Valluri, W. Chanmanee, N. D. Tacconi, W. A. Wampler, W. Y. Lin, T. F. Carlson, V. Ramani, and K. Rajeshwar, *J. Chem. Sci.*, **121**, 655 (2009).
25. J. Tian, G. Sun, M. Cai, Q. Mao, and Q. Xin, *J. Electrochem. Soc.*, **155**, B187 (2008).
26. G. Benke and W. Gnot, *Hydrometallurgy*, **64**, 205 (2002).
27. D. C. Johnson, D. T. Napp, and S. Bruckenstein, *Electrochim. Acta*, **15**, 1493 (1970).
28. S. Mitsushima, Y. Koizomi, K. I. Ota, and N. Kamiya, *Electrochem. Commun.*, **75**, 155 (2007).
29. D. A. J. Rand and J. Woods, *J. Electroanal. Chem. Interfacial Electrochem.*, **35**, 209 (1972).
30. A. J. Arvia, J. C. Canullo, E. Custidiano, C. L. Perdriel, and W. E. Triaca, *Electrochim. Acta*, **31**, 1359 (1986).
31. J. C. Canullo, W. E. Triaca, and A. J. Arvia, *J. Electroanal. Chem. Interfacial Electrochem.*, **200**, 397 (1986).
32. W. A. Egli, A. Visintin, W. E. Triaca, and A. J. Arvia, *Appl. Surf. Sci.*, **68**, 583 (1993).
33. K. I. Ota, S. Nishigori, and N. Kamiya, *J. Electroanal. Chem. Interfacial Electrochem.*, **257**, 205 (1988).
34. X. Wang, R. Kumar, and D. Myers, *Electrochem. Solid-State Lett.*, **9**, A225 (2006).
35. V. O. Mittal, H. R. Kunz, and J. M. Fenton, *ECS Trans.*, **3**(1), 507 (2006).
36. W. Liu and M. Crum, *ECS Trans.*, **3**(1), 531 (2006).
37. W. Liu and M. Crum, *ECS Trans.*, **3**(1), 541 (2006).
38. M. Aoki, H. Uchida, and M. Watanabe, *ECS Trans.*, **3**(1), 485 (2006).
39. B. Lakshmanan, W. Huang, D. Olmeijer, and J. W. Weidner, *Electrochem. Solid-State Lett.*, **6**, A282 (2003).
40. M. Inaba, T. Kinomoto, M. Kiriake, R. Umebayashi, A. Tasaka, and Z. Ogumi, *Electrochim. Acta*, **51**, 5746 (2006).
41. K. Teranishi, K. Kawata, S. Tsushima, and S. Hirai, *Electrochem. Solid-State Lett.*, **9**, A475 (2006).
42. R. M. Darling and J. P. Meyers, *J. Electrochem. Soc.*, **150**, A1523 (2003).
43. R. M. Darling and J. P. Meyers, *J. Electrochem. Soc.*, **152**, A242 (2005).
44. J. P. Meyers and R. M. Darling, *J. Electrochem. Soc.*, **153**, A1432 (2006).
45. G. Selvarani, S. Vinod Selvaganesh, S. Krishnamurthy, G. V. M. Kiruthika, P. Sridhar, S. Pitchumani, and A. K. Shukla, *J. Phys. Chem. C*, **113**, 7461 (2009).
46. U.S. DOE, Cell Component Accelerated Stress Test Protocols for PEM Fuel Cells, March 2007.
47. R. Woods, in *Electroanalytical Chemistry*, A. J. Bard, Editor, Marcel Dekker, New York (1976).
48. S. G. Neophytides, K. Murase, S. Zafeiratos, G. Papakonstantinou, F. E. Paloukis, N. V. Krstajic, and M. M. Jaksic, *J. Phys. Chem. B*, **110**, 3030 (2006).
49. F. Kodera, Y. Kuwahara, A. Nakazawa, and M. Umeda, *J. Power Sources*, **172**, 698 (2007).
50. S. J. Tauster, S. C. Fung, and R. L. Garten, *J. Am. Chem. Soc.*, **100**, 170 (1978).
51. L. Brewer, *Science*, **161**, 115 (1968).
52. M. M. Jakšić, *Electrochim. Acta*, **29**, 1539 (1984).
53. S. J. Tauster, S. C. Fung, R. T. K. Baker, and J. A. Horsley, *Science*, **217**, 121 (1981).
54. D. E. Curtin, R. D. Lousenberg, T. J. Henry, P. C. Tangeman, and M. E. Tisack, *J. Power Sources*, **131**, 41 (2004).
55. A. Jańczyk, A. W. Głubisz, K. Urbanska, H. Kisch, G. Stochel, and W. Macyk, *Free Radic Biol. Med.*, **44**, 1120 (2008).
56. P. Tengvall, H. Elwinga, L. Sjöqvista, I. Lundströma, and L. M. Bjurstenb, *Biomaterials*, **10**, 118 (1989).

Downloaded 22 Jun 2010 to 210.212.252.226. Redistribution subject to ECS license or copyright; see http://www.ecsdl.org/terms_use.jsp